Available online at www.sciencedirect.com
SCIENCE DIRECT
Acta Materialia 54 (2006) 2463–2471
Acta MATERIALIA
www.actamat-journals.com

High-energy X-ray measurements of structural anisotropy and excess free volume in a homogenously deformed Zr-based metallic glass

R.T. Ott [a,*], M.J. Kramer [a,b], M.F. Besser [a], D.J. Sordelet [a]

[a] *Materials and Engineering Physics Program, 105 Metals Development, Ames Laboratory (USDOE) Iowa State University, Ames, IA 50011, USA*
[b] *Materials Science and Engineering Department, Iowa State University, Ames, IA 50011, USA*

Received 26 September 2005; received in revised form 20 January 2006; accepted 23 January 2006
Available online 20 March 2006

Abstract

We have used high-energy X-ray scattering to measure the structural anisotropy and excess free volume in a homogeneously deformed Zr-based metallic glass alloy. The scattering results show that bond length anisotropy is present in the samples following isothermal tensile creep deformation. The average atomic bond length in the direction parallel to the tensile loading axis is larger than that in the direction normal to the loading axis. The magnitude of the bond length anisotropy is found to be dependent on the gradient of macroscopic plastic strain along the gauge length. Furthermore, the scattering results show that the excess free volume also increases with increasing macroscopic plastic strain. Results from differential scanning calorimetry analysis of free volume variations along the gauge length of the creep samples are consistent with results from the X-ray scattering experiments.

Keywords: Metallic glasses; Creep; X-ray diffraction; Differential scanning calorimetry

1. Introduction

At low temperatures and high applied stresses, plastic deformation in metallic glasses is inhomogeneous wherein the plastic strain is localized into shear bands. Inhomogeneous flow occurs by a deformation-induced disordering of the atomic structure characterized by a shear-induced dilation in the localized regions of deformation [1–5]. The dilation that accompanies plastic deformation in metallic glasses is commonly described in terms of the free volume model [6,7] in which the strain rate is expressed as

$$\dot{\varepsilon} = 2c_f k_f \frac{\varepsilon_0 v_0}{\Omega} \sinh\left(\frac{\sigma \varepsilon_0 v_0}{2kT}\right) \quad (1)$$

where σ is the applied stress, c_f is the flow defect concentration, k_f is a temperature-dependent constant, ε_0 is the local strain, v_0 is the localized shear region volume, Ω is the atomic volume, k is Boltzmann's constant, and T is the temperature. In this treatment, the flow defects are described as density fluctuations with a volume that exceeds some threshold value, v^*. The defect creation rate has previously been reported to be dependent on the applied stress [7], strain rate [8,9], and the product of the stress and strain rate [10,11].

At higher temperatures and lower applied stresses, metallic glasses deform in a homogeneous manner. Several studies on glasses deformed at high stresses in the homogenous flow region have also confirmed the presence of strain-induced structural disordering through the observation of a drop in the flow stress for constant strain rate experiments [8,9] and accelerating strain rates for constant-stress creep experiments [12,13]. This strain-induced structural disordering leads to an increase in the excess free volume present. A competing ordering process referred to as structural relaxation also occurs during homogeneous deformation, which acts to annihilate excess free volume [9,14]. Therefore, in order to prevent structural relaxation from negating the free volume creation, creep experiments are often performed at high applied stresses. Recently,

* Corresponding author. Tel.: +1 515 294 3616; fax: +1 515 294 8727.
E-mail address: rtott@ameslab.gov (R.T. Ott).

1359-6454/$30.00
doi:10.1016/j.actamat.2006.01.026

Yavari and coworkers have utilized synchrotron X-ray scattering to measure the excess free volume in metallic glass ribbons after deformation [15,16]. Although they measured the excess free volume in inhomogeneously deformed glasses, the technique is also applicable to homogeneously deformed alloys.

In addition to measuring excess free volume, X-ray scattering has also been utilized to examine structural anisotropy in homogeneously deformed metallic glasses [17,18]. By comparing the diffraction spectra with the scattering vector parallel and perpendicular to the tensile loading axis, Egami and coworkers determined that the total structure factor was anisotropic for the two directions [17,18]. The pair distribution function calculated from the anisotropic structure factor revealed that the number of bonds in the direction normal to the loading axis increases while the number of bonds in the direction parallel to the loading axis decreases. This anisotropic atomic structure, which they referred to as bond orientational anisotropy, was also observed using molecular dynamics simulations [19]. The results of these experiments and simulations suggest that metallic glasses retain directional memory of the plastic deformation.

In this paper, we report using high-energy synchrotron X-ray scattering to examine structural anisotropy and excess free volume creation in a Zr-based metallic glass deformed by isothermal creep. The structural anisotropy and excess free volume were measured along the gauge length of the creep samples as a function of the macroscopic plastic strain. Moreover, we examined the dependence of the amount of excess free volume on the plastic strain using differential scanning calorimetry (DSC). The effects of the strain localization near the fracture tip on the structural anisotropy and the excess free volume are discussed.

2. Experimental

2.1. Isothermal creep experiments

Metallic glass alloys of composition $Zr_{41.2}Ti_{13.8}Cu_{12.5}Ni_{10}Be_{22.5}$ were cut using an electro-discharge machine (EDM) into standard "dogbone" samples with a gauge section $12.7 \times 5 \times 3$ mm (see Fig. 1). Creep experiments were performed in uniaxial tension at 598 K, which is nominally 25 K below the glass transition temperature of the alloy, for 300 h. For each creep test the applied load was held constant, thus allowing the true stress to change during loading since the cross-sectional area changed during deformation. To account for structural relaxation that occurs at the testing temperature, a stress-free companion sample from the same alloy was placed in the creep rig with each creep sample. After completion of the creep tests, the cross-sectional areas along the gauge lengths of the samples were measured to calculate the amount of macroscopic plastic strain. For the X-ray experiments, a slice, approximately 0.6 mm thick, of each creep sample was EDM cut parallel to the longitudinal direction (in the plane parallel to the page) defined in Fig. 1. The cut faces were polished to a final finish with 0.05 μm alumina paste to remove the EDM marks and other surface artifacts and to obtain parallel faces for the X-ray studies.

2.2. High-energy X-ray scattering

Synchrotron X-ray experiments were performed at the MUCAT (6-IDD) beamline of the advanced photon source at Argonne National Laboratory. Silicon double-crystal monochromators were employed to select an X-ray energy of 130 keV for the experiments, which were performed in transmission mode. A MAR 345 digital image plate with a 100×100 μm pixel size was positioned 530 mm downstream from the samples to record the scattered intensity. The samples were mounted in a 4-circle goniometer on a translation stage with their flat surfaces normal to the incident beam so that scans could be obtained along different regions of the gauge length parallel to the longitudinal (loading) direction (see Fig. 1). A beam size of 0.4×0.4 mm was used to ensure that unique regions of material were sampled along the gauge length. For all of the samples, the camera length and beam center were determined by fitting the pattern obtained from NIST Si standard 640C using FIT2D software [20].

A major advantage of using a two-dimensional area detector is the ability to separate out structural information in the longitudinal (Q parallel to the tensile loading axis) and the transverse (Q normal to the loading axis) directions, where Q is the wave momentum number ($Q = 4\pi\sin\theta/\lambda$). For this purpose, the intensity was integrated radially with respect to ϕ, where ϕ is the angle that Q sweeps out on the image plate. In this case, the 3 o'clock position on the image plate corresponds to $\phi = 0°$. The intensity as a function of Q for a given radial bin is expressed as

$$I^{\phi}(Q) = \int_{\phi_1}^{\phi_2} I(Q,\phi)\,\mathrm{d}\phi \tag{2}$$

where ϕ_1 and ϕ_2 represent the start and end angle of a particular radial bin. For the data analysis, the full pattern was rebinned into 60 radial bins each with a width of 6°. The intensities for the longitudinal and the transverse directions were taken as the average of three radial bins for a total bin size of 18°. Because a two-dimensional detector was used in the experiments, six radial bins were actually used for each direction since the bins 180° from each other were also integrated in order to help minimize errors associated with defining the beam center [21]. Scans at different positions along the gauge length were obtained by translating the sample up and down in the beam. For each position, 3–6 scans were recorded to obtain better counting statistics. A typical diffraction pattern recorded on the digital image plate is shown in Fig. 2(a) along with the binned region that was used for integration of the scattered intensity in

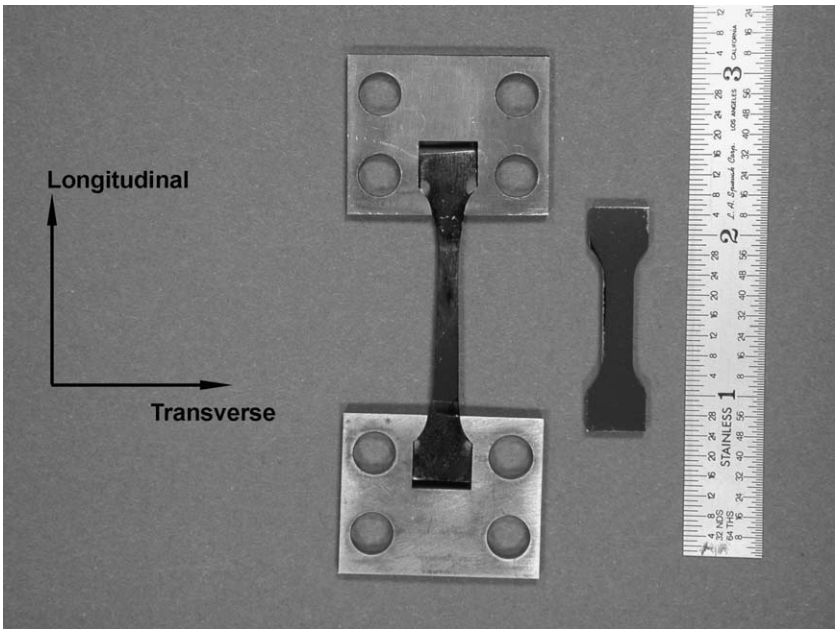

Fig. 1. Typical sample before and after isothermal creep experiment performed in tension. The longitudinal and transverse directions are shown. Note the large elongation in the sample after loading.

the longitudinal direction (see Fig. 2(b)). The patterns for the creep samples show only broad diffuse scattering features at every position, which is consistent with an amorphous structure. The selected Q-region that was used for fitting is noted by the vertical dashed lines. The first diffuse scattering peak was fit with a Voigt function (see Fig. 2(c)) in order to estimate the Q-value at the centroid of the fitted peak from diffraction patterns collected at each selected position along the gauge length of the creep sample.

2.3. DSC measurements

To examine the effects of homogeneous deformation on the thermal behavior of the alloy and thereby compare the amount of plastic strain with the amount of excess free volume, DSC measurements were performed under flowing nitrogen using a Perkin–Elmer Pyris 7 instrument. Samples were cut from different regions along the gauge length of the same test piece used in the X-ray scattering experiments. A heating rate of 0.67 K/s and a cooling rate of 1.67 K/s were used for all of the measurements. The samples were heated to 973 K in order to obtain a fully crystallized structure. For a baseline correction, a second scan of the crystallized sample was subtracted from the first scan.

3. Results and discussion

3.1. Structural anisotropy

As shown in Fig. 1, the cross-sectional area of the creep samples decreases with increasing distance from the sample grip as a result of necking. Since the cross-section changes along the gauge length, the true stress also varies along the gauge length for constant load tests. Heggen and coworkers [11] have noted the importance of knowing the true stress during a test rather than just the nominal stress; therefore, creep experiments are often performed in compression with a strain feedback loop in order to keep the applied stress constant. Such a technique provides a means of eliminating geometric artifacts from the experiments when examining strain rate changes. For our experiments, however, a gradient of strains (stresses) along the gauge length was intentionally produced for the X-ray characterization. Given that the structural changes being probed with the X-rays are not much larger than the sensitivity of the technique, experimental artifacts need to be minimized. For the X-ray scattering experiments, sample alignment, specifically variance in the camera length, is one of the largest sources of errors in the data. A small change in the camera length can have a significant effect on the measured peak positions. For creep experiments performed in compression at a constant stress, each different strain level would require mounting a new sample in the goniometer to be X-rayed. Small changes in the camera length for each sample could introduce large uncertainties into the data. Therefore, we chose to perform the creep experiments in uniaxial tension, which allows us to vary the strain (stress) along the gauge length, while maintaining a constant camera length.

To examine the structural anisotropy that develops following homogenous deformation, we compared the diffraction spectra obtained from the longitudinal (parallel to loading axis) and transverse (normal to loading axis) directions of the creep samples. Fig. 3 shows the intensity difference plots, $\Delta I(Q)$, where

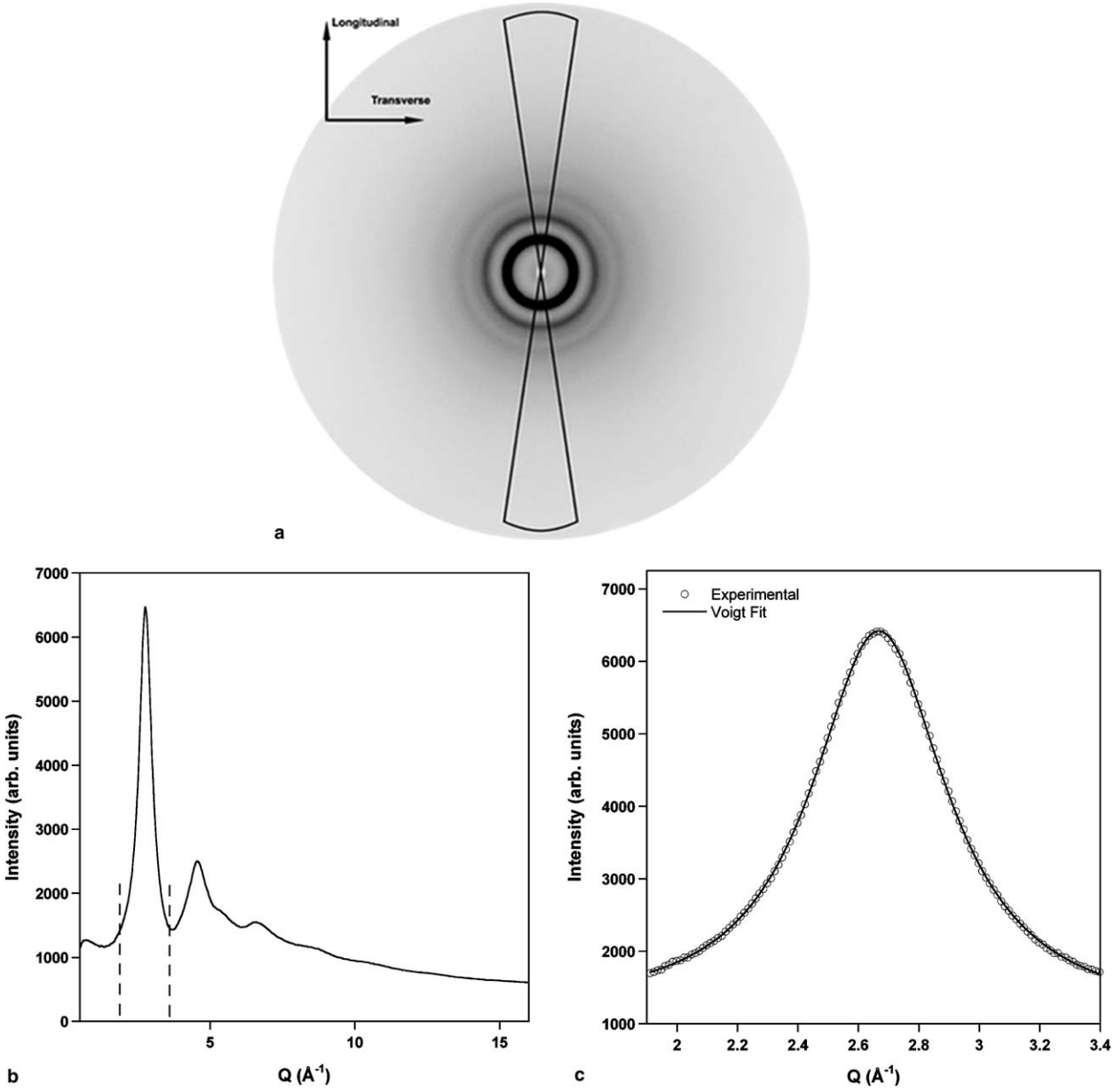

Fig. 2. (a) Typical diffraction pattern from homogenously deformed sample. The slices represent the 18° bins that were integrated to obtain the diffraction pattern for the longitudinal direction of the sample, which is shown in (b). The region of the pattern that was fit with a Voigt peak is denoted by the dashed lines. (c) Voigt fit of first scattering maxima.

$$\Delta I(Q) = I(Q)_{\text{long}} - I(Q)_{\text{trans}} \tag{3}$$

for one point along the gauge length of the creep sample and the companion sample. The intensity difference plot for the creep sample (see Fig. 3(a)) shows a clear difference in the positions of the first scattering maxima for the longitudinal and transverse directions. However, beyond the first peak, the structural anisotropy is less clear. To improve the quality of the data beyond the first scattering maxima, we can incorporate the intensity difference plot for the companion sample according to

$$\Delta I(Q)_{\text{corr}} = \Delta I(Q)_{\text{creep}} - \Delta I(Q)_{\text{comp}} \tag{4}$$

where $\Delta I(Q)_{\text{comp}}$ is the intensity difference plot for the companion sample and $\Delta I(Q)_{\text{corr}}$ is the corrected intensity difference plot for the creep sample. As mentioned above, the companion sample was not loaded during the creep tests, and thus should not exhibit any anisotropy. Therefore, any features in the intensity difference plot for the companion sample should be due to experimental artifacts that arise from small variances in the beam optics, area detector, sample mounting, etc. The corrected intensity difference plot for the creep sample (see Fig. 3(c)) clearly shows the structural anisotropy that exists beyond the first scattering peak. The results illustrate that both the first and

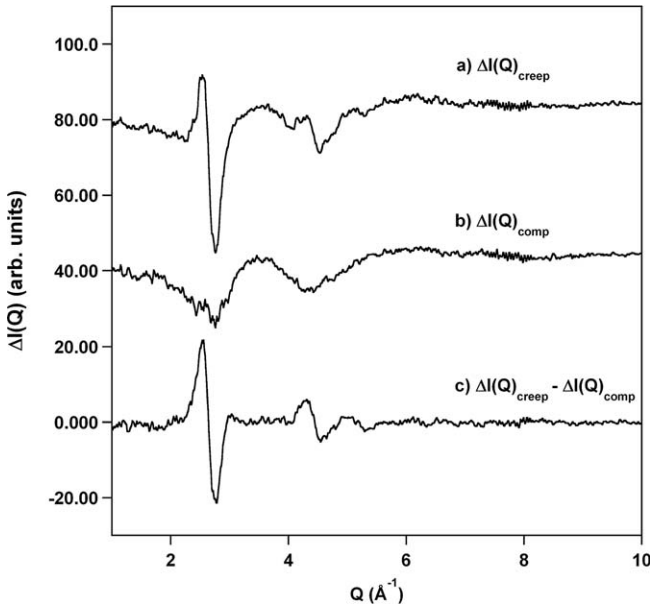

Fig. 3. Intensity difference plots calculated by subtracting $I(Q)_{\text{trans}}$ from $I(Q)_{\text{long}}$ for the (a) $\sigma_0 = 250$ MPa creep sample and (b) companion sample. (c) Corrected intensity difference plot for the creep sample.

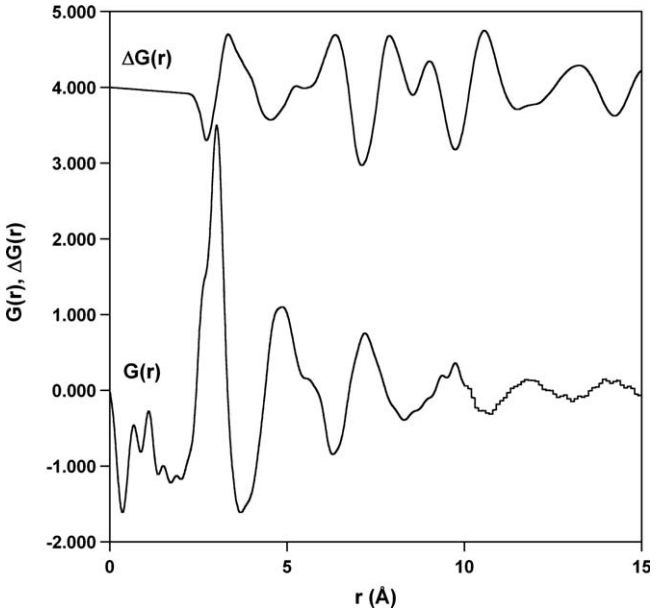

Fig. 4. Anisotropic reduced pair distribution function, $\Delta G(r)$, along with the isotropic reduced pair distribution function, $G(r)$, for the creep sample loaded at an initial stress of 250 MPa. The curve for $\Delta G(r)$ has been offset for clarity.

second peaks in the pattern from the longitudinal direction are shifted to lower Q-positions relative to the transverse direction. It should be pointed out that while the difference in Q-positions of the peaks for the two directions is consistent with an anisotropic atomic structure, Q is not a real materials property, but rather is related to the average atomic spacing. To obtain real space information regarding the atomic structure, we calculated the anisotropic total structure factor according to

$$\Delta S(Q) = \frac{\Delta I(Q)_{\text{corr}}}{N\langle f(Q)\rangle^2} \tag{5}$$

where N is the number of atoms and $f(Q)$ is the compositionally averaged atomic scattering factor. Since the experiments are performed in transmission mode, the absorption, multiple scattering, and Compton scattering in the longitudinal and transverse directions should be equivalent, and thus can be ignored. The anisotropic total structure factor, $\Delta S(Q)$, was smoothed with a Savitsky–Golay function and the high-Q data were forced to 0 with an appropriate damping function. The anisotropic reduced pair distribution function, $\Delta G(r)$, was then obtained by Fourier transformation of $\Delta S(Q)$ as follows:

$$\begin{aligned}\Delta G(r) &= 4\pi r[\Delta\rho(r) - \Delta\rho_0] \\ &= \frac{2}{\pi}\int_0^\infty Q[\Delta S(Q)]\sin(Qr)\,\mathrm{d}Q\end{aligned} \tag{6}$$

The anisotropic reduced pair distribution function along with the isotropic $G(r)$, which was calculated from the total structure factor obtained from integration of the full 360° diffraction pattern, are shown in Fig. 4. The presence of peaks in the anisotropic reduced pair distribution function, $\Delta G(r)$, indicates that the nearest-neighbor distances in the longitudinal and transverse directions are different ($\Delta G(r)$ would be a straight line for equivalent nearest-neighbor distances in the two directions). More specifically, the results show that the bond length in the longitudinal direction is larger than the bond length in the transverse direction. The similar magnitude of the shifts of the peaks in $\Delta G(r)$ relative to the peaks in $G(r)$ is consistent with a uniform increase in the average bond length in the longitudinal direction as compared to the transverse direction. The anisotropy seen in the real space data is in good agreement with the reciprocal space data, suggesting that the differences in the peak positions in reciprocal space can be used for examining the structural anisotropy. However, the reciprocal space data can only be used to examine qualitatively the structural anisotropy since the higher order interactions are not taken into account.

We further examined the effects of the macroscopic plastic strain on the structural anisotropy in the creep samples by fitting the first scattering maxima (in reciprocal space) for the longitudinal and transverse directions for scans taken from specific regions along the gauge length. The fitted peak positions as function of the plastic strain, calculated from reduction in the cross-sectional area, for the creep samples loaded at initial uniform stresses of 250 and 400 MPa are shown in Fig. 5(a) and (b), respectively. For convenience, we will refer to the samples as $\sigma_0 = 250$ and $\sigma_0 = 400$ MPa. The range of the plastic strains for the $\sigma_0 = 400$ MPa sample is larger than that for the $\sigma_0 = 250$ MPa sample because a larger region of its gauge length was examined, i.e., scans were taken closer to the sample grip. For both creep samples, the measured Q-position of the first scattering peak in the longitudinal direction

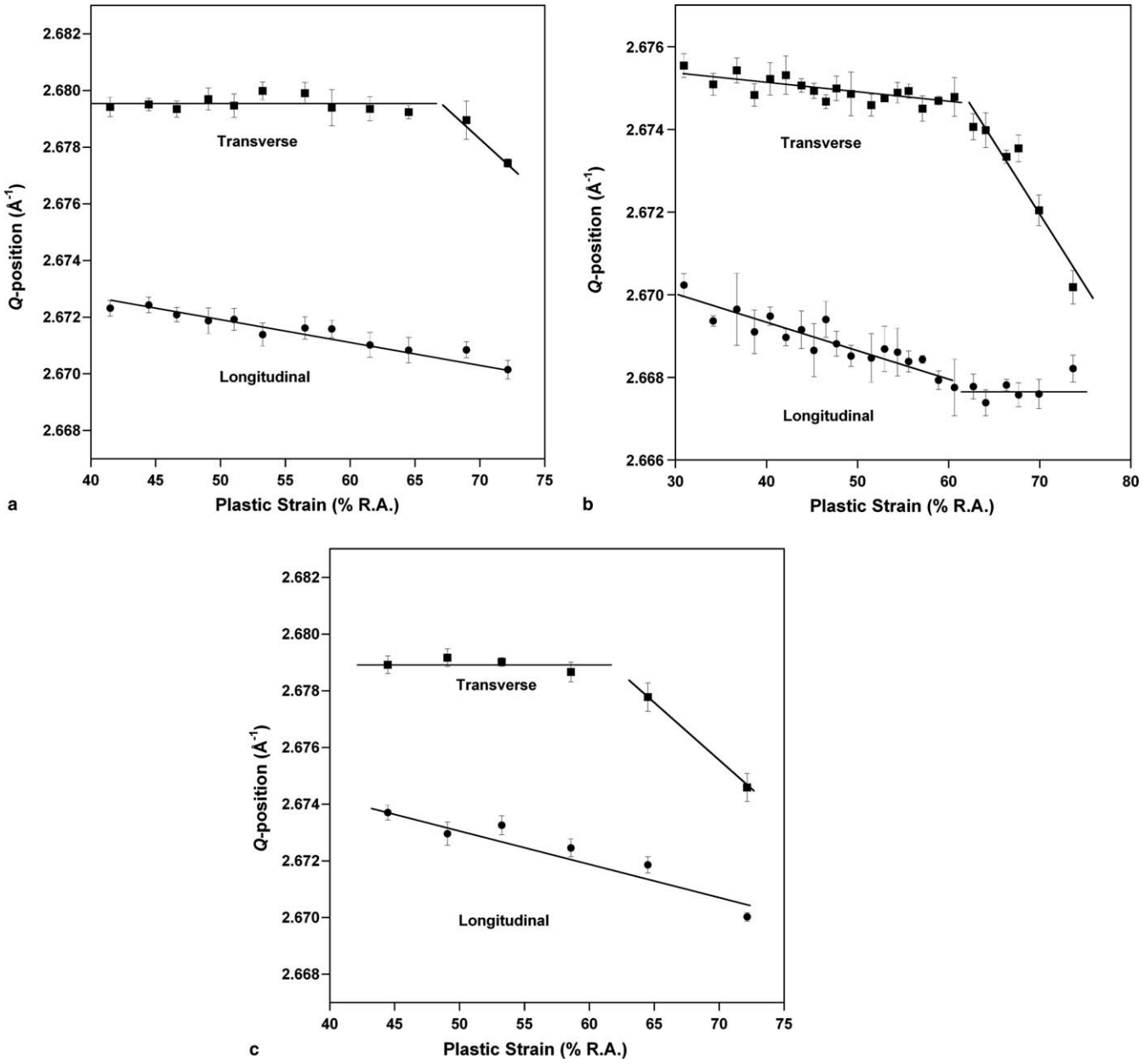

Fig. 5. Measured peak position of the first scattering maxima in the longitudinal and transverse sample directions as a function of plastic strain for creep samples loaded at initial stresses of (a) 250 and (b) 400 MPa. (c) Measured peak positions for creep sample loaded at an initial stress of 250 MPa that has been rotated 90° relative to the beam and image plate so that longitudinal sample direction correlates to transverse camera direction.

is smaller than that in the transverse direction, which is consistent with a larger average atomic bond length in the longitudinal direction. It should be noted that the X-ray measurements were performed on the creep samples after unloading; therefore, the anisotropy in the bond lengths is not caused by elastic strain [22]. To determine if the differences in the peak positions for the longitudinal and transverse directions of the samples were an artifact of the experimental conditions, we rotated the goniometer 90° so that the orientation of the longitudinal and transverse directions of the $\sigma_0 = 250$ MPa sample were rotated relative to the incident X-ray beam and the digital image plate. Fig. 5(c) shows similar anisotropy in the measured peak positions for the longitudinal and transverse directions along the gauge length, indicating that the directional dependence of the average bond length is not an experimental artifact.

As shown in Fig. 5, the degree of structural anisotropy in both creep samples increases with increasing plastic deformation for strains below ~60%. However, for plastic strains above 60%, the bond length anisotropy significantly decreases. The transition to decreasing anisotropy with increasing plastic strain corresponds to the region along the gauge lengths where the macroscopic plastic strain becomes more localized. Fig. 6 shows the macroscopic plastic strain, which was measured from the reduction in

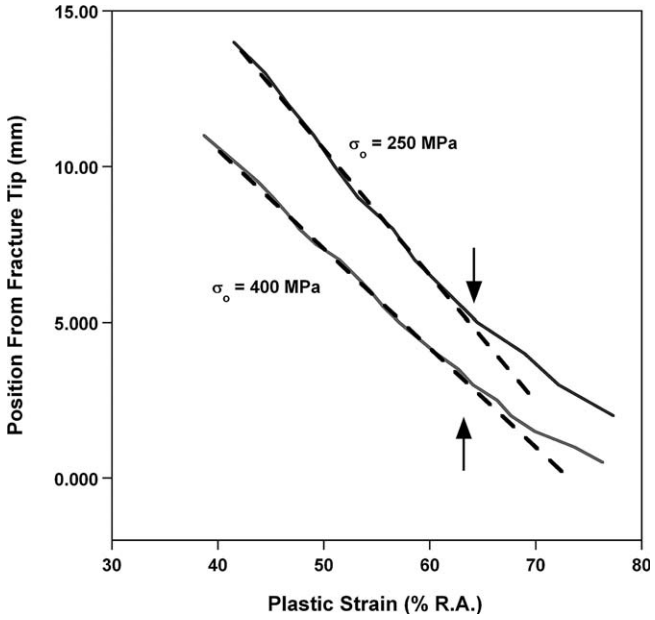

Fig. 6. Macroscopic plastic strain measured from the reduction in cross-sectional area (% RA) as function of position along gauge length. The arrows indicate where the plastic strain deviates from linearity (dashed lines) and the strain becomes more localized.

cross-sectional area, as a function of distance from the fracture tip; the two samples investigated in this work fractured near the center of the deformed region during removal from the creep furnace. For plastic strains below ~60%, the plastic strain scales linearly with the distance along the gauge length. However, above 60%, the plastic stain as a function of position along the gauge length deviates from linearity, indicating that the strain has become more localized near the fracture tip. The results for the two creep samples suggest that an increase in the localization of the plastic strain leads to a decrease in the degree of bond length anisotropy, which while unexpected, is perhaps consistent with previous work done on Pd-based glasses. Safarik and coworkers [23] localized the homogeneous deformation in cube-shaped samples by putting a through-hole in the center of the sample. The center hole in the samples caused the strain to be localized into bands emanating from the hole edges. For cycled loading, they found that the test pieces exhibited no directional memory of the previous plastic deformation, suggesting that the atomic structure did not exhibit any significant anisotropy after each loading event. While the strain localization in our experiment is less dramatic, the decrease in structural anisotropy with increasing localization appears to be in agreement with their results. The reason for the apparent decrease in anisotropy is currently under investigation.

3.2. Excess free volume measurements

To measure the excess free volume present in the samples after homogeneous deformation, we followed an approach similar to that proposed by Yavari and coworkers who calculated the free volume in inhomogeneously deformed metallic glass ribbons by measuring the peak position (in reciprocal space) of the first scattering maxima as a function of temperature before and after heating through the glass transition temperature [15,16]. In their study, the excess free volume was calculated according to

$$\Delta V_{\mathrm{f}} = \frac{\left[\left(\frac{Q(T^0)}{Q(T)}\right)^3_{(\mathrm{up1})} - \left(\frac{Q(T^0)}{Q(T)}\right)^3_{(\mathrm{up2})}\right]}{\left(\frac{Q(T^0)}{Q(T)}\right)^3_{(\mathrm{up2})}} \tag{7}$$

where up1 is the first heating cycle up to the glass transition, and up2 is the second heating cycle to the glass transition temperature after the sample has been cycled through the glass transition temperature and cooled back down to the reference temperature (T^0). Since our experiments were performed at room temperature, the peak positions of the creep samples were compared to the peak position of the companion sample from each creep test. As mentioned above, the companion samples have an identical thermal history to the creep samples, and thus should be representative of structural relaxation that occurred during the tests. For amorphous materials, the average bond length, d, is related to the peak position of the first scattering maxima, Q, according to

$$d = k\frac{2\pi}{Q} \tag{8}$$

where k is a constant related to the atomic structure. From Eq. (8), the excess free volume in the creep samples can be calculated by

$$\Delta V_{\mathrm{f}} = \frac{d^3_{\mathrm{creep}} - d^3_{\mathrm{comp}}}{d^3_{\mathrm{comp}}} = \frac{\left(\frac{1}{Q_{\mathrm{creep}}}\right)^3 - \left(\frac{1}{Q_{\mathrm{comp}}}\right)^3}{\left(\frac{1}{Q_{\mathrm{comp}}}\right)^3} \tag{9}$$

where Q_{comp} and Q_{creep} are the peak positions of the first scattering maxima for the companion and creep samples, respectively. For calculating the excess free volume, we assume that the average bond lengths in the two transverse directions of the samples are equivalent, and thus

$$\left(\frac{1}{Q}\right)^3_{\mathrm{comp,creep}} = \left(\frac{1}{Q_{\mathrm{long}}}\right)\left(\frac{1}{Q_{\mathrm{trans}}}\right)^2 \tag{10}$$

for the creep and companion samples in Eq. (8). Fig. 7 shows the calculated excess free volume in the two creep samples as a function of macroscopic plastic strain. For both samples, the excess free volume measured along the gauge length increases with increasing plastic strain. The magnitude of the excess free volume is consistent with reported values for inhomogeneously deformed metallic glasses measured by in situ X-ray scattering [15]. Similar to the bond length anisotropy, the measured excess free volume also exhibits a marked change for plastic strains greater than 60%. However, unlike the structural anisotropy, which decreases with increasing plastic strains above 60%, the excess free volume exhibits a large increase with

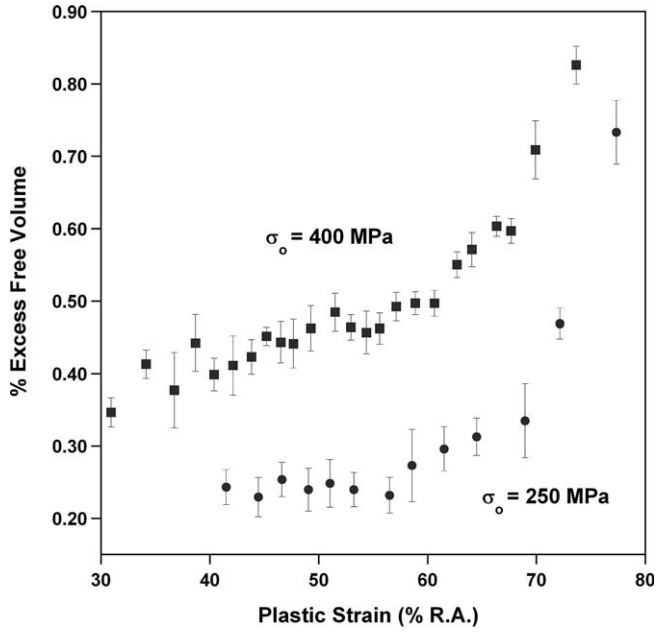

Fig. 7. Measured excess free volume in the creep samples as a function of the macroscopic plastic strain for samples loaded at initial stresses of 250 and 400 MPa.

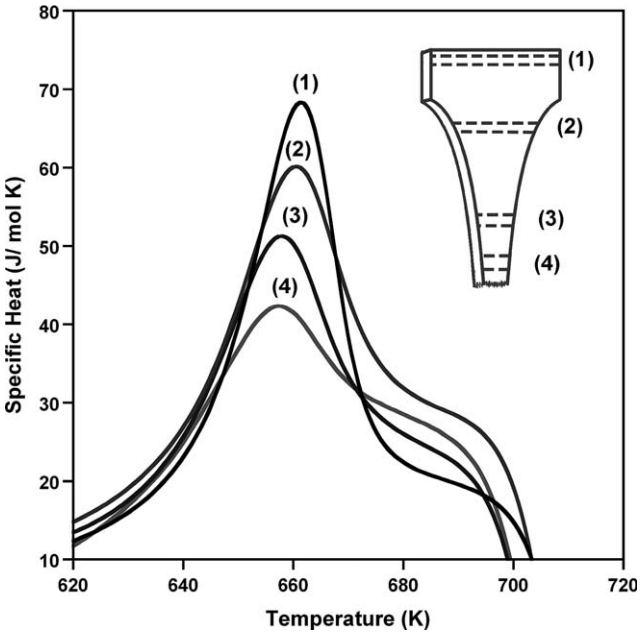

Fig. 8. DSC plots of the region around the glass transition temperature for the $\sigma_0 = 400$ MPa creep sample. The positions along the gauge length from which the samples were taken are shown in the inset.

increasing plastic strain in this region. As shown in Fig. 6, the macroscopic strain becomes more localized for these higher plastic strains. This suggests that the increase in strain localization strongly promotes dilation in the creep samples.

3.3. DSC measurements

The change in free volume creation throughout the creep samples was further examined by performing constant-rate DSC on thin samples cut from different regions within the grip section and along the gauge length. Fig. 8 shows the DSC scans near the glass transition temperature for the $\sigma_0 = 400$ MPa sample; the accompanying schematic indicates the approximate positions where the samples were cut from the creep sample. The magnitude of the endothermic heat signal associated with the glass transition phenomenon is lowest for the sample taken from near the heavily deformed tip and highest for the sample taken from the undeformed sample grip. It has been previously reported for metallic glasses that the height of the glass transition peak decreases as the amount of free volume present increases [8,24–27]. As shown in Fig. 6, the macroscopic plastic strain increases along the gauge length with the maximum strain occurring at the fracture tip. The DSC results illustrate that the height of the glass transition peak decreases as the plastic strain increases, and thereby the excess free volume is increasing with increasing plastic strain. This is consistent with the X-ray scattering results, which also show that the excess free volume in the creep samples is dependent on the level of strain along the gauge length.

4. Conclusions

We have examined the structural anisotropy and excess free volume in a Zr-based metallic glass alloy after homogeneous thermomechanical deformation. The anisotropic nature of the average bond length following deformation was seen by shifts in the scattering peaks in reciprocal space and shifts in the peaks of the reduced pair distribution function in real space. Furthermore, the scattering results show that both the structural anisotropy and the excess free volume increase with increasing plastic strain for strains less than ~60%. Relaxation studies using DSC further confirm that the amount of excess free volume is dependent on the gradient of plastic strain along the gauge length. For plastic strains above 60%, the magnitude of the bond length anisotropy exhibits a large decrease while the excess free volume exhibits a large increase. The large change in the two quantities at the higher plastic strains corresponds to the regions along the gauge lengths where the macroscopic plastic strain is more localized.

Acknowledgements

We gratefully acknowledge D. Rehbein for performing the creep experiments and F. Spaepen, S.B. Biner, A.R. Yavari, and E. Üstündag for helpful discussions and comments. This work was performed for the US Department of Energy by Iowa State University under Contract No. W-7405-Eng-82. The high-energy X-ray work at the MUCAT sector of the APS was supported by the US Department of Energy, Office of Science, Basic Energy Sciences under Contract No. W-31-109-Eng-38.

References

[1] Spaepen F, Taub AI. In: Luborsky FE, editor. Flow and fracture in amorphous metallic alloys. London: Butterworths; 1983. p. 231.
[2] Chen HS, Chuang SY. Appl Phys Lett 1975;27:316.
[3] Cahn RW, Pratten NA, Scott MG, Sinning HR, Leonardson L. Mater Res Soc Symp Proc 1984;28:241.
[4] Donovan PE, Stobbs WM. Acta Metall 1981;29:1419.
[5] Li J, Spaepen F, Hufnagel TC. Philos Mag A 2002;82:2623.
[6] Spaepen F, Turnbull D. Scripta Metall 1974;8:563.
[7] Spaepen F. Acta Metall 1977;25:407.
[8] Hey PD, Sietsma J, Van Den Beukel A. Acta Mater 1998;46:5873.
[9] Lu J, Ravichandran G, Johnson WL. Acta Mater 2003;51:3429.
[10] Falk ML, Langer JS. Phys Rev E 1998;57:7192.
[11] Heggen M, Spaepen F, Feuerbacher M. J Appl Phys 2005;97:033506.
[12] Heggen M, Spaepen F, Feuerbacher M. Mater Sci Eng A 2004;375–377:366.
[13] Heggen M, Spaepen F, Feuerbacher M. Mater Res Soc Symp Proc 2004;805:MM7.2.1.
[14] Taub AI, Spaepen F. Acta Metall 1980;28:1781.
[15] Hajlaoui K, Benameur T, Vaughan G, Yavari AR. Scripta Mater 2004;51:843.
[16] Yavari AR, Moulec AL, Inoue A, Nishiyama N, Lupu N, Matsubara E, et al. Acta Mater 2005;53:1611.
[17] Suzuki Y, Haimovich J, Egami T. Phys Rev B 1987;35:2162.
[18] Egami T, Dmowski W, Kosmetatos P, Boord M, Tomida T, Oikawa E, et al. J Non-Cryst Solids 1995;192–193:591.
[19] Tomida T, Egami T. Phys Rev B 1993;48:3048.
[20] Hammersley AP, Svensson SO, Hanfland M, Fitch AN, Hausermann D. High Press Res 1996;14:235.
[21] Korsunsky AM, Wells KE, Withers PJ. Scripta Mater 1998;39:1705.
[22] Poulsen HF, Wert JA, Neufeind J, Honkimaki V, Daymond M. Nat Mater 2005;4:22.
[23] Safarik DJ, Cady CM, Schwarz RB. Acta Mater 2005;53:2193.
[24] Beukel Avd, Sietsma J. Acta Metall Mater 1990;38:383.
[25] Daniel BSS, Reger-Leonhard A, Heilmaier M, Eckert J, Schultz L. Mech Time-Depend Mat 2002;6:193.
[26] Slipenyuk A, Eckert J. Scripta Mater 2004;50:39.
[27] Martin SW, Walleser J, Karthikeyan A, Sordelet DJ. J Non-Cryst Solids 2004;349:347.